Astron. Astrophys. 359, 1042–1058 (2000)

ASTRONOMY AND ASTROPHYSICS

The chemical evolution of hot white dwarfs in the presence of diffusion and mass loss

K. Unglaub and I. Bues

Dr. Remeis-Sternwarte Bamberg, Astronomisches Institut der Universität Erlangen-Nürnberg, Sternwartstrasse 7, 96049 Bamberg, Germany

Received 14 March 2000 / Accepted 9 May 2000

Abstract. We present the results of new diffusion calculations with mass loss for hot white dwarfs with $T_{\rm eff} > 50000$K. In contrast to previous calculations, the stellar parameters $T_{\rm eff}$, $\log g$ and the mass loss are allowed to vary. With stellar parameters from evolutionary tracks and two independent estimates of the mass loss rates the time-dependance of the composition during the cooling is investigated in an outer region of about $10^{-4} M_*$. With an improved numerical method the elements H, He, C, N and O can be taken into account simultaneously.

In the $T_{\rm eff}$ - $\log g$ -diagram we expect a DAO/DA transition region near an approximately horizontal line characterized by $\log g \approx 7$. In hydrogen-rich objects with lower surface gravities helium lines should be detectable, because mass loss with $\dot{M} \geq 10^{-12} M_*/{\rm y}$ prevents or retards the gravitational settling of helium. PG 1159 stars are predicted to evolve into DO's when the surface gravity reaches a value between $\log g = 7.5$ and 8.0 and the mass loss rate decreases below about $10^{-13} M_*/{\rm y}$. From the results we suggest the existence of an evolutionary link between PG 1159 stars and most of the DO's. Calculations with various admixtures of hydrogen in PG 1159 stars show that most DAO's cannot be descendants of hydrogen-poor PG 1159 stars with a number ratio ${\rm H/He} \leq 0.1$, because mass loss is expected to retard the floating up of hydrogen. The majority of hot DAO's and DA's must be descendants of hydrogen-rich precursors.

Key words: stars: abundances – stars: evolution – diffusion – stars: white dwarfs

1. Introduction

The model atmosphere analyses of hot white dwarfs with effective temperatures $T_{\rm eff} \geq 50000$K revealed a variety of surface compositions. There are helium-, carbon- and oxygen-rich PG 1159 stars (Dreizler & Heber 1998), helium-rich DO's analyzed by Dreizler & Werner (1996) and Dreizler (1999), hydrogen-rich DAO's analyzed by Bergeron et al. (1994) and Napiwotzki (1999) with various abundances of helium and the DA's in which no helium can been detected, whereas traces of heavy elements may be present (e.g. Holberg et al. 1999; Koester et al. 1998). For a long time the question has been debated if these different compositions are preferably due to events which occur before the star evolves into a white dwarf (primordial scenario) or if the surface compositions are a consequence of processes, which occur on the cooling sequence (see the review of Fontaine & Wesemael 1997). Because of the lack of hydrogen-rich pre-white dwarfs, Fontaine & Wesemael (1987) suggested that most white dwarfs descend from helium-rich progenitors with some minor amounts of hydrogen mixed in their envelope. During the cooling hydrogen diffuses upwards. So the star evolves via the DAO stage with a stratified H/He atmosphere into a DA. After the detection of hydrogen-rich pre-white dwarfs and even "hybrid" objects with about similar abundances of hydrogen and helium (e.g. Napiwotzki & Schönberner 1991, 1995; Rauch et al. 1999) there is now clear observational evidence that pre-white dwarfs may have a variety of H/He ratios. In addition, from an analysis of helium line profiles Napiwotzki & Schönberner (1993) and Bergeron et al. (1994) ruled out the existence of stratified atmospheres for most of the DAO's.

From standard theory of stellar evolution, only the existence of hydrogen-rich white dwarfs is expected. The masses of the outer hydrogen layer and the helium-rich intershell region on top of the C/O interior may depend on the total stellar mass. For $M_* = 0.6 M_\odot$ a hydrogen layer mass of about $10^{-4} M_*$ is predicted (Blöcker et al. 1997). As a possible explanation for the existence of H-deficient post-AGB stars the born-again AGB-star scenario originally developped by Iben et al. (1983) was proposed. A very late thermal pulse experienced by a white dwarf during its early cooling phase brings it back onto the AGB where mass loss may remove the H-rich envelope. After the inclusion of hydrodynamically based overshoot into the AGB model calculations, Herwig et al. (1999) have shown that due to the additional energy release from convective H-burning a convective instability reaches up to the surface. This produces a H-deficient and C-O-rich surface chemistry. The most recent results are summarized in Blöcker (2000).

There is clear observational evidence that not all properties of the white dwarfs surface chemistry can be explained by this scenario. Additional processes must exist, which operate when the star is already on the cooling sequence and change the surface composition. The existence of the DB-gap requires that all helium-rich white dwarfs evolve into hydrogen-rich ones until

Send offprint requests to: K. Unglaub
(unglaub@sternwarte.uni-erlangen.de)

they have cooled down to $T_{\rm eff} \approx 45000$K. The lower limit for PG 1159 stars is at $T_{\rm eff} \approx 70000$K (Dreizler & Heber 1998). Therefore C und O must be removed from the surface regions. The most extensively investigated effects are gravitational settling possibly counteracted by radiative levitation (Chayer et al. 1995a,b and references therein). However, various phenomena cannot be explained with the assumption of an equilibrium between both effects. For example, the predicted helium abundances in DAO's are clearly too low (Vennes et al. 1988). In PG 1159 stars carbon and oxygen would sink in time scales of 1000y only (Unglaub & Bues 1997). Therefore we investigated the influence of mass loss (Unglaub & Bues 1998; Paper I). The results have been quite promising. For a DAO with $T_{\rm eff} = 80000$K, $\log g = 7.0$ and a mass loss rate of the order 10^{-13} to $10^{-12}{\rm M}_*/{\rm y}$, the surface abundance of helium decreases from ${\rm He/H} = 0.1$ to 10^{-3} within a time scale of 10^6y. So in the presence of a weak wind the time scales of gravitational settling may be of the same order of magnitude as the cooling ages. In Unglaub & Bues (1999) we have shown that in PG 1159 stars winds with $\dot{M} > 10^{-14}$ (in the following we give the mass loss rates in $M_*/{\rm y}$ and omit the units) considerably retard or prevent the gravitational settling of the heavy elements.

In comparison to Paper I, the most important improvement of the present investigation is, that $T_{\rm eff}$, $\log g$ and the mass loss rate are allowed to vary during the calculations. So the cooling of the star can be taken into account quantitatively. This new aspect and the involved physics are summarized in Sect. 2. In Sect. 3 the numerical method is described in detail. As it is more stable than the one used in Paper I, the elements H, He, C, N and O can be simultaneously taken into account for all calculations.

In Sect. 4 we discuss the existence of winds and various estimates of the mass loss rates from a theoretical point of view. Winds have been detected in hydrogen-rich central stars of planetary nebulae (Kudritzki et al. 1997; Perinotto 1993) and in luminous PG 1159 stars (Koesterke et al. 1998; Koesterke & Werner 1998). The mass loss rates are of the order 10^{-9} to 10^{-6}. Thus we expect that in these phases of stellar evolution the effect of gravitational settling is still negligible. For hot white dwarfs there is some evidence for the existence of winds. Werner et al. (1995) and Dreizler et al. (1995a) detected absorption lines of highly ionized stages of several elements in some DO's and one DAO and suggest that they are formed in a rapidly accelerating wind (Werner et al. 1999). However, $T_{\rm eff}$ and $\log g$ of these objects are not yet known. Holberg et al. (1998a,b) report on the detection of detached, blue shifted features in the majority of hot DO's and in a few DA's. These features are possibly formed in circumstellar matter, which may be due to episodes of mass loss. From these observational results it seems that winds are more likely to exist in DO's rather than in DA's.

In Sects. 5, 6 and 7 we investigate the chemical evolution of white dwarfs on the cooling sequence starting from a given composition, which in the following will be denoted as initial composition. The computations start, when or just before the star enters the cooling sequence. Here the expected mass loss rates are large enough so that diffusion processes cannot yet have changed the surface composition significantly. In principle, the initial compositions may vary from star to star. In hydrogen-rich pre-white dwarfs, Méndez (1991) found evidence for a variety of carbon abundances. A detailed NLTE analysis of such objects is in progress, first results have been obtained for the case of iron. (Deetjen et al. 1999). Because of this poor knowledge of the initial composition, we assume solar ratios He/H and CNO/H. The results are presented in Sect. 5. We especially investigate the question, for which hot hydrogen-rich white dwarfs the presence of helium can be expected and when do DAO's transform into DA's. Close inspection of the element abundances in hydrogen-deficient post-AGB stars shows that each object has its individual He/C/N/O mixture (Werner 2000). In Sect. 6 we consider a typical case with an initial composition ${\rm C/He} = 0.3$, ${\rm N/He} = 0.01$ and ${\rm O/He} = 0.1$ (number ratios) and discuss the evolutionary link between PG 1159 stars and DO's. In Sect. 7 for the case of PG 1159 with various admixtures of hydrogen, the transformation of helium-rich into hydrogen-rich white dwarfs is investigated. Finally, in Sect. 8 we summarize the most important results and discuss the existence of chemically stratified atmospheres and the origin of the DB-gap.

2. Basic assumptions

The most important improvement in comparison to Paper I is, that the stellar parameters are allowed to vary. $T_{\rm eff}$ and $\log g$ as a function of time are taken from evolutionary tracks, $\dot{M}$ is estimated as described in Sect. 4. Thus the effect of cooling on the stellar structure can be taken into account. We neglect, however, the possible effect of the changing composition on the stellar parameters and the cooling ages. This would require the implementation of the method into a stellar evolution code. As nuclear burning is not taken into account, the calculations are restricted to the outer regions. The inner boundary of our computation domain, characterized by a fixed gas pressure scale, is at $P_{\rm g} = 10^{16}$Pa. As during the cooling the gravity increases, the mass within the computation domain decreases. For $\log g = 7.5$ it is about $10^{-4} M_*$. The composition at the inner boundary is held fixed. As we know from our previous results, usually the diffusion time scales at this depth are large in comparison to the cooling ages of about 10^6y. An exception may be the case with traces of hydrogen in a helium-rich background plasma. In addition, for typical mass loss rates of the order $10^{-12} M_*/{\rm y}$ and cooling ages of 10^6y the total mass loss is small compared to the mass within the computation domain. Thus we expect that the inner boundary condition has negligible influence on the predicted surface composition. At the beginning of the calculations, that is just before the pre-white dwarfs enter the cooling sequence, the composition within the computation domain is assumed to be homogeneous.

The temperature structure is obtained from

$$\frac{dT}{dr} = -\frac{3}{16} T_{\rm eff}^4 \overline{\chi} \frac{1}{T^3} \frac{R_*^2}{r^2} \tag{1}$$

with $T^4 = \frac{1}{2} T_{\rm eff}^4$ at the outer boundary. In contrast to Paper I radial effects are taken into account now. To account for the effect

of the composition on the temperature structure we calculate monochromatic continuum opacities as described in Unglaub & Bues (1996), from which the Rosseland mean opacity $\overline{\chi}$ is evaluated. Eq. (1) is a sufficient approximation for our purposes. For the mass loss rates of interest the matter of the stellar atmosphere is removed within a few years or even less. Within this time diffusion cannot change the composition significantly. Then the atmosphere is replaced by matter from underlying regions. Therefore in diffusion calculations with mass loss especially the conditions in deeper regions are important. This is in contrast to calculations without mass loss, where the surface abundance can be predicted only if the radiative accelerations in the stellar atmosphere are known.

The radiative accelerations for heavy elements are obtained as described in Unglaub & Bues (1996) with the method and line list similar as in Vauclair et al. (1979). For He^+ and H the evaluation of the line profiles has been improved (see Paper I). For hydrogen-like ions the factor f_{ion} from Massacrier (1996) is taken into account. With this factor the momentum transferred to the heavy particles in photoionization processes is calculated as described in Paper I. For the mass loss rates and stellar parameters of interest only the radiative accelerations for helium- and hydrogenlike ions of the CNO elements are of major importance. Lower ionization states are preferably present in the outermost regions near the stellar atmosphere. As explained above, the conditions in these regions have little influence on our results, however.

The diffusion velocities v_{d} are calculated as in Unglaub & Bues (1997) from the system of linear equations, which consists of the various momentum equations and the condition of zero net mass flow. For an element l the momentum equation reads

$$-\frac{dp_l}{dr} - n_l m_l g_{(r)} + n_l \overline{Z}_l e E + n_l F_{l,\mathrm{rad}} = \sum_t K_{l,t}\left(v_{\mathrm{d},t} - v_{\mathrm{d},l}\right). \tag{2}$$

The expressions on the left represent the momentum per unit volume and unit time transferred to the element by the gradient of the partial pressure, gravity, the electric field E and the radiative force $F_{l,\mathrm{rad}}$. Ionization effects and thermal diffusion are neglected. The former may be of importance only in regions of partial ioniziation and thus are negligible at least for H and He. Paquette et al. (1986a,b) have shown that for plasma conditions typical for hot white dwarfs thermal diffusion is less effective than gravitational settling. For our calculations the relative magnitude of the diffusion velocity and the drift velocity due to mass loss (see Eq. (3)) is of special importance. If, for example, the inward diffusion velocity of an element would be larger by a factor of two, this could be compensated by an increase of the mass loss rate by a similar factor. As the mass loss rates are obtained from rough estimates, these simplifications in the diffusion calculations seem to be justified. The dependence of the gravity g on the distance r from the stellar center is approximated by $g_{(r)} \approx \frac{GM_*}{r^2}$. The resistance coefficients $K_{l,t}$ are obtained according to Paquette et al. (1986a). The charge $\overline{Z}_l$ of an element is the mean value over all ionization states.

Although we take into account mass loss, the total stellar mass is assumed to be constant. This is justified, because for the considered mass loss rates and time scales the total mass loss is negligible in comparison to M_*. With this assumption the mean velocity due to mass loss can be obtained from the equation of continuity:

$$v_{\mathrm{w}} = \frac{\dot{M}}{4\pi r^2}\frac{1}{\rho} \tag{3}$$

where ρ is the density and v_{w} the wind velocity.

3. Numerical method

In this section we describe the complete numerical method. It is more stable and more accurate than the one used in Paper I and allows to take into account H, He, C, N and O simultaneously in all calculations. The stability of the methods used requires that the Courant condition is fulfilled. If Δr is the geometrical distance between two grid points, v the velocity and Δt the time step-width, then the relation $\Delta r \leq v\Delta t$ must be valid. Therefore we use a primary grid (described in Sect. 3.1) for the construction of the $T - P_{\mathrm{g}}$ stratification and for each element a variable secondary grid (Sect. 3.2) for the diffusion and mass loss calculations. The spacing of the secondary grids are such that the Courant condition holds.

At each point of the fixed gas pressure scale we would like to calculate the time-derivative of the mass fraction of an element l. The mass-fraction is defined as

$$X_l = \frac{A_l m_{\mathrm{p}} n_l}{\rho}. \tag{4}$$

A_l is the atomic weight, m_{p} the proton mass and ρ the density. The mass fraction may change because of the effects of diffusion and wind. The corresponding variation of the particle density will be denoted as $\left(\frac{dn_l}{dt}\right)^{(\mathrm{d+w})}$. Mass loss and diffusion do not change ρ, because the wind velocity is derived from the equation of continuity (see Sect. 2) and diffusion does not lead to a net mass flow. However, the stellar structure changes with time. For example, if the gravity increases the mass-depth at a given gas pressure decreases. So mass elements move to larger values on the P_{g} scale. In the presence of concentration gradients, this leads to variations of the composition at the various points on the P_{g} scale. We denote the corresponding time-variation of the mass-fraction with $\left(\frac{dX_l}{dt}\right)^{(\mathrm{evol})}$. Alltogether we then have

$$\frac{dX_l}{dt} = \frac{A_l m_{\mathrm{p}}}{\rho}\left(\frac{dn_l}{dt}\right)^{(\mathrm{d+w})} + \left(\frac{dX_l}{dt}\right)^{\mathrm{evol}}. \tag{5}$$

For the particle density and the total velocity v of an element, in the following we omit the indices l:

$$\frac{dn}{dt} \equiv \left(\frac{dn_l}{dt}\right)^{(\mathrm{d+w})} \tag{6}$$

$$v = v_{\mathrm{d},l} + v_{\mathrm{w}}. \tag{7}$$

$\frac{dn}{dt}$ is obtained from the equation of continuity for radial symmetry:

$$\frac{dn}{dt} = -\frac{1}{r^2}\frac{d\left(nvr^2\right)}{dr}. \tag{8}$$

This equation has to be evaluated numerically for each element. Under certain conditions, which are fulfilled preferably in the outer regions, we use a modified upwind scheme described in Sect. 3.3. Otherwise the monotonic transport scheme described in Sect. 3.4 is used.

The variation of the mass fraction due to the stellar evolution is written as

$$\left(\frac{dX_l}{dt}\right)^{\mathrm{evol}} = \frac{dX_l}{dm}\frac{dm}{dt}. \tag{9}$$

m is the mass depth, $\frac{dm}{dt}$ is the time variation of the mass depth at a given point on the P_{g} scale. The numerical evaluation of Eq. (9) is described in Sect. 3.5. The boundary conditions and the time integration are described in Sects. 3.6 and 3.7. Then we will briefly comment on the stability of the method.

In the following subsections some conventions are used. The indices i and j, which denote the points of the primary and the secondary grid, respectively, are defined such that they are 1 at the outer boundary and increase to the stellar interior. The geometrical depth variable r, however, is the distance from the stellar center and thus increases in opposite direction. The velocities and flows have a positive sign if they are directed to the stellar surface.

3.1. The primary grid

For the calculation of the $T - P_{\mathrm{g}}$ stratification a grid is constructed as described in Unglaub & Bues (1997). For the gas pressure at the outer and inner boundaries we chose $2000\mathrm{Pa}$ and $10^{16}\mathrm{Pa}$, respectively. The grid spacing is

$$P_{\mathrm{g}(i+1)} \approx P_{\mathrm{g}(i)} + 0.1 * P_{\mathrm{g}(i)}. \tag{10}$$

The points denoted as $i\mathrm{b}$ in Unglaub & Bues (1997) define the primary grid of the present calculations. At each grid point the diffusion and wind velocities are calculated.

3.2. The secondary grid

Let $v_{\mathrm{d}(i)}$ and $v_{\mathrm{w}(i)}$ be the diffusion and wind velocities for a given element at the points of the primary grid and $r_{(i)}$ the distance of point i from the stellar center. With Δt_0 we denote the chosen time step-width. It is not necessarily identical with the actual time step-width which may be smaller (see Sect. 3.7). These points of the primary grid which are simultaneously points of the secondary grid are found from the following condition:

$$\sum_{i=i_{(j)}}^{i_{(j+1)}} \frac{r_{(i)} - r_{(i+1)}}{v_{\mathrm{w}(i)} + |v_{\mathrm{d}(i)}|} \leq \Delta t_0 \leq \sum_{i=i_{(j)}}^{i_{(j+1)}+1} \frac{r_{(i)} - r_{(i+1)}}{v_{\mathrm{w}(i)} + |v_{\mathrm{d}(i)}|}. \tag{11}$$

The expression $i_{(j)}$ represents the relation between the indices j of the secondary grid and the indices i of the primary grid. The outer boundary of the primary grid is per definition a point of the secondary grid, so that $i_{(1)} = 1$. The left inequality is our numerical representation of the Courant condition. The time which the flow needs to proceed from point j to $j+1$ must be smaller than Δt_0. In other words, the distance the flow proceeds during a time step must be smaller than the distance between two grid points. In addition we demand that at least in the outer regions $v\Delta t$ is of the same order of magnitude as Δr. This is the meaning of the second inequality. This additional condition improves the accuracy in the regions where the modified upwind scheme is used.

The points j represent zone centers. At these points the time derivations of the number densities $\frac{dn}{dt}$ will be evaluated. The inner and outer boundaries of the zone j will be denoted with $j + \frac{1}{2}$ and $j - \frac{1}{2}$, respectively. To evaluate the various quantities like velocity or radius at the zone boundaries, let us consider the following expression:

$$i_{(j+1/2)} = \frac{1}{2}\left(i_{(j)} + i_{(j+1)}\right). \tag{12}$$

If $i_{(j+1/2)}$ is an integer, then the quantities at this point of the primary grid are taken. Let, however, $i_{(j+1/2)}$ be $k + \frac{1}{2}$, where k is an integer. In this case the mean values of the quantities at the points k and $k+1$ of the primary grid are used. So the point $j + \frac{1}{2}$ is exactly at the geometrical center of the points j and $j+1$ only if the primary and secondary grids are identical.

3.3. The modified upwind scheme

At a grid point j the modified upwind scheme is used if the following two conditions are fulfilled. $J = nv$ denotes the flow of the considered species of particles.

$$J_{(j-1)} > 0 \wedge J_{(j)} > 0 \wedge J_{(j+1)} > 0 \tag{13}$$

$$i_{(j+1)} - i_{(j)} > 1 \vee i_{(j)} - i_{(j-1)} > 1. \tag{14}$$

The first condition means, that the flows at point j as well as at the two neighbouring points must have a positive sign: they are directed to the stellar surface. The second condition means that near point j the primary and secondary grid are not identical. Both conditions are fulfilled preferably in the outer regions, where the wind velocity is large in comparison to the diffusion velocities and where during one time step the flow covers a distance which is larger than the distance between two points of the primary grid.

Now we denote with $\frac{dN}{dt}$ the number of particles per unit time which cross a surface $4\pi r^2$. Then $\frac{dN}{dt}_{(j+1/2)}$ is the number of particles per unit time, which enter the zone j via its inner boundary and $\frac{dN}{dt}_{(j-1/2)}$ is the corresponding number which leave the zone via the outer boundary. We use the numerical representations

$$\frac{dN}{dt}_{(j+1/2)} = n_{(j+1)} v_{(j+1)} 4\pi r^2_{(j+1)} \tag{15}$$

$$\frac{dN}{dt}_{(j-1/2)} = n_{(j)} v_{(j)} 4\pi r^2_{(j)}. \tag{16}$$

The obvious method would be to evaluate the values n, v and r at the zone boundary. This is numerically unstable, however. In the usual upwind scheme only the particle density n is evaluated upstream, whereas the velocities are evaluated at the zone boundaries. This would be very unconvenient for our purposes, because in the outer regions n and v may vary by order of magnitudes between the grid points. The particle flows, however, are similar at the various grid points, at least if the composition gradient is not too large. For this reason we evaluate all quantities upstream. The time derivative of the particle density of an element at point j is obtained from

$$\frac{dn}{dt}_{(j)} = \frac{\frac{dN}{dt}_{(j+1/2)} - \frac{dN}{dt}_{(j-1/2)}}{4\pi r^2_{(j)} \Delta r_{(j)}}. \tag{17}$$

The expression in the denominator on the right would be the volume of the zone j, if $\Delta r_{(j)} = r_{(j-1/2)} - r_{(j+1/2)}$ were used. However, we use

$$\Delta r_{(j)} = r_{(j)} - r_{(j+1)}. \tag{18}$$

This is more consistent with our upwind evaluation of r in Eqs. (15) and (16).

3.4. The monotonic transport scheme

The monotonic tranport scheme (abbreviated mono scheme) is used, if the conditions (13) and (14) are not fulfilled. This is the case especially in the inner regions, where the primary and the secondary grid tend to be identical. The basic ideas from which the mono scheme is derived are described in Hawley et al. (1984). It is an improved upwind scheme, which combines stability with accuracy. In deep regions, during one time step the flow covers a distance which is small in comparison to the distance between two points of the primary grid, so that $v\Delta t_0 \ll \Delta r$. Especially in such cases the mono scheme is more accurate than the upwind scheme.

According to the mono scheme the flow at the zone boundary $j + \frac{1}{2}$, for example, is evaluated as follows:

$$\text{if} \quad v_{(j+1/2)} \geq 0 \quad \text{then} \quad J_{(j+1/2)} = v_{(j+1/2)} \times \left(n_{(j+1)} + \left(\frac{dn}{dr}\right)_{(j+1)} \frac{1}{2} \left(\Delta r_{(j)} - v_{(j+1/2)} \Delta t_0\right) \right) \tag{19}$$

$$\text{if} \quad v_{(j+1/2)} < 0 \quad \text{then} \quad J_{(j+1/2)} = v_{(j+1/2)} \times \left(n_{(j)} - \left(\frac{dn}{dr}\right)_{(j)} \frac{1}{2} \left(\Delta r_{(j)} + v_{(j+1/2)} \Delta t_0\right) \right). \tag{20}$$

$\Delta r_{(j)}$ is the geometrical distance between the points j and $j+1$ as defined in Eq. (18). In a similar way the flow $J_{(j-1/2)}$ at the outer zone boundary is obtained. The mono scheme requires the knowledge of the time step. However, we fix Δt after the time derivatives $\frac{dn}{dt}$ for the various elements have been calculated. Therefore we must use the Δt_0, which is equal or larger than Δt (see Sect. 3.7). The spatial derivative $\frac{dn}{dr}$ at a point j is evaluated similar as in Hawley et al. (1984):

$$a = \frac{n_{(j-1)} - n_{(j)}}{r_{(j-1)} - r_{(j)}}, \; b = \frac{n_{(j)} - n_{(j+1)}}{r_{(j)} - r_{(j+1)}}$$

$$c = \frac{n_{(j-1)} - n_{(j+1)}}{r_{(j-1)} - r_{(j+1)}}$$

$$\frac{dn}{dr}_{(j)} = 0 \qquad \text{if} ab \leq 0$$
$$\frac{dn}{dr}_{(j)} = \frac{ab}{c} \qquad \text{else.} \tag{21}$$

For $\frac{dn}{dr} = 0$ the mono scheme is identical with the upwind scheme. With the flows $J_{(j+1/2)}$ and $J_{(j-1/2)}$ at the inner and outer zone boundaries, respectively, the number of particles crossing the boundaries per unit time are obtained according to:

$$\frac{dN}{dt}_{(j+1/2)} = J_{(j+1/2)} 4\pi r^2_{(j+1/2)} \tag{22}$$

$$\frac{dN}{dt}_{(j-1/2)} = J_{(j-1/2)} 4\pi r^2_{(j-1/2)}. \tag{23}$$

Then the time derivative of the particle density of an element at point j is

$$\frac{dn}{dt}_{(j)} = \frac{\frac{dN}{dt}_{(j+1/2)} - \frac{dN}{dt}_{(j-1/2)}}{4\pi r^2_{(j)} \left(r_{(j-1/2)} - r_{(j+1/2)}\right)}. \tag{24}$$

3.5. The evaluation of $\left(\frac{dX_l}{dt}\right)^{(\mathrm{evol})}$

To evaluate the variation of the mass fraction of an element l, which is due to changes of the mass depth at a given point, according to Eq. (9) we need numerical representations of $\frac{dX}{dm}$ and $\frac{dm}{dt}$. Here m is the mass depth and X is the mass fraction of an element (the index l is omitted). At a point j we use the obvious representation:

$$\frac{dX}{dm}_{(j)} = \frac{X_{(j+1)} - X_{(j-1)}}{m_{(j+1)} - m_{(j-1)}}. \tag{25}$$

An exception is the point $j$max which represents the inner boundary. Here is used:

$$\frac{dX}{dm}_{(j\max)} = \frac{X_{(j\max)} - X_{(j\max-1)}}{m_{(j\max)} - m_{(j\max-1)}}. \tag{26}$$

The variation of the mass depth during the considered time step is obtained by linear extrapolation from the preceding time step with

$$\frac{dm}{dt}_{(j)} = \frac{m^{(t)}_{(j)} - m^{(t-1)}_{(j)}}{\Delta t^{(t-1)}}. \tag{27}$$

$\Delta t^{(t-1)}$ is the width of the preceding time step. The nominator on the right represents the difference between the actual mass depth at point j and the corresponding mass depth in the preceding model.

3.6. Boundary conditions

The outermost points of the primary and secondary grid are identical. The point $i = j = 1$ represents the center of the

outermost zone. The outer boundary of this zone is beyond of our computation domain. The gas pressure at $j = 1$ is $2000\mathrm{Pa}$ for all our computations. Therefore the density will be low enough, so that for the considered mass loss rates the wind velocity is usually large in comparison to the diffusion velocities. As shown in Paper I this tends to smooth out concentration gradients. This justifies the assumption of homogeneous composition in the region between the two outermost grid points:

$$X_{\mathrm{l}(j=1)} = X_{\mathrm{l}(j=2)}. \tag{28}$$

This choice avoids numerical problems at the outermost point. At the lower boundary ($j = j\mathrm{max}$) at $P_{\mathrm{g,max}} = 10^{16}\mathrm{Pa}$, we assume that diffusion and mass loss do not change the mass fractions. Only if the mass depth at j_{max} decreases, the composition is allowed to vary. In this case mass elements located within our computation domain at $P_{\mathrm{g}} < P_{\mathrm{g,max}}$ move to the lower boundary. So we obtain the inner boundary condition:

$$\begin{aligned} \frac{dX_l}{dt}_{(j\mathrm{max})} &= 0 \quad \text{if} \quad \frac{dm}{dt}_{j(\mathrm{max})} \geq 0 \quad \text{and} \\ \frac{dX_l}{dt}_{(j\mathrm{max})} &= \frac{dX_l}{dm}_{(j\mathrm{max})} \frac{dm}{dt}_{(j\mathrm{max})} \quad \text{else.} \end{aligned} \tag{29}$$

3.7. The time step

In Sect. 3.2 we have introduced the chosen time step width Δt_0. This value is used to define the secondary grids for the various elements and to obtain the time derivatives of the particle densities according to the monotonic transport scheme. For all calculations presented in this paper $\Delta t_0 = 1\mathrm{y}$ is used. The drawback of the numerical method is, that during many time steps the composition fluctuates around some slowly changing mean value. To restrict these fluctuations, during one time step we do not allow the mass fractions to vary by more than 2%. For each element l at each grid point j we define

$$\Delta t_{l,j} = 0.02 X_{l,(j)} \left| \frac{dX_l}{dt}_{(j)} \right|^{-1}. \tag{30}$$

$\Delta t_{l,j}$ is the time, for which the mass fraction would change by 2%. The actual time step width used in the computations is the minimum value of Δt_0 and all $\Delta t_{l,j}$:

$$\Delta t = \min\left(\Delta t_0, \Delta t_{l,j}\right). \tag{31}$$

In most cases Δt and Δt_0 are identical. Exceptions may occur, if one of the elements has an extremely low abundance or during the calculations for helium-rich white dwarfs with traces of hydrogen. Then Δt may be smaller than Δt_0. The new mass fractions of the element l at the points j of the secondary grid are obtained according to

$$\left(\frac{dX_l}{dt}\right)^{(t+\Delta t)}_{(j)} = X^{(t)}_{l(j)} + \frac{dX_l}{dt}_{(j)} \Delta t. \tag{32}$$

The new mass fractions of these points i of the primary grid, which are not points of the secondary grid, are obtained from interpolation. Then a new model is constructed. The various velocities and particle densities and the secondary grids are updated after each time step. Other quantities like opacities, radiative accelerations per particle and mass loss rates are updated only if the mass fraction of at least one element has changed by at least 10% at one of the grid points.

3.8. The stability of the method

The method is by far more stable than the one used in Paper I. There the stable upwind scheme has been used only for the part of the flow which is due to the wind, whereas the diffusion flows have been evaluated at the zone boundaries. Then unstabilities occurred in cases of very large diffusion velocities. This may happen for extremely low abundances, where the radiative acceleration may be much larger than the gravitational one. Therefore in the present method stable schemes are used for the total flow. If the velocities increase the grid is adapted by increasing the distances between the points. We use a separate grid for each element. So if one element requires a coarse grid (because of large velocities), the grids for the other elements can be kept more refined, which means a better accuracy. However, numerical instabilities may still occur under certain circumstances. This is for the case of helium-rich white dwarfs with small admixtures of hydrogen ($\mathrm{H/He} \leq 10^{-3}$ by number).

4. Estimate of the mass loss rates

To estimate the mass loss rates in white dwarfs, in the discussion of Paper I we used a formula from Blöcker (1995) derived from the calculations of Pauldrach et al. (1988) for hot central stars of planetary nebulae.

$$\dot{M} = 1.29 * 10^{-15} L^{1.86} \qquad [M_\odot/y]. \tag{33}$$

In Paper I has been shown that with the corresponding mass loss rates the separation of hot hydrogen-rich white dwarfs into DAO's and DA's can be explained. However, the use of this equation for white dwarfs may be criticized for the following reasons. First, it does not take into account the dependance of the mass loss rate on the composition. This dependance is of special importance for our calculations. Secondly, Eq. (33) yields a nonzero mass loss rate for all white dwarfs and thus disregards the existence of a wind limit. Thirdly, the Pauldrach et al. results for hot CSPN have been obtained with their improved CAK (Castor et al. 1975) theory. However, for extremely weak winds expected in white dwarfs the CAK theory is probably not the appropriate one. This is due to the effect of line shadowing discussed by Babel (1996) for the case of main sequence B stars. Whereas dense winds are driven by a large number of weak lines, in thin winds the strong lines contribute significantly to the radiative acceleration. These are, however, affected by their broad photospheric counterparts. As a consequence the radiative acceleration does not only depend on the density and the gradient of the velocity as in the CAK theory, but on the velocity itself in addition. This effect may lead to mass loss rates, which may be lower by more than a factor of ten as predicted by the CAK theory. An additional problem is, that extremely weak

winds may be selective, so that only these elements are lost for which the radiative acceleration is large enough. The problem of selective winds has been investigated for A stars by Babel (1995). For similar reasons Abbott's (1982) mass loss formula cannot be expected to be reliable for the case of white dwarfs. Moreover, it is valid for $T_{\rm eff} \leq 50000$K only.

For purposes of comparison, Eq. (33) will be applied in some cases. In addition we use an alternative estimate of $\dot{M}$ as described below. It is simple enough to be implemented into our code. The intention is to allow for a dependence of $\dot{M}$ on the chemical composition, to recognize when the wind limit is reached and to make the calculations formally consistent. The effect of line shadowing would require model atmosphere calculations, however.

The existence of a chemically homogeneous, radiatively driven wind requires that the maximum possible radiative acceleration is at least equal to the gravitational acceleration. If this is the case, we estimate $\dot{M}$ from the conditions at the sonic point by use of various approximations, which will be described in this section. For an isothermal wind with constant mean particle mass μ the equation for the wind velocity v can be written as (e.g. Mihalas 1978):

$$v\frac{dv}{dr}\left(1-\frac{a^2}{v^2}\right) = -g + g_{\rm rad,C} + g_{\rm rad,L} + \frac{2a^2}{r} \qquad (34)$$

where g, $g_{\rm rad,C}$, $g_{\rm rad,L}$ are the gravitational acceleration and the radiative accelerations due to bound-free transitions and lines, respectively. a is the isothermal sound velocity. At the sonic point, where $v = a$, the right hand side must be zero. In "cool" winds with $T \approx T_{\rm eff}$ the expression $\frac{2a^2}{r}$ at the sonic point is small, so that the total radiative acceleration must approximately be equal to g. In radiatively driven winds the sonic point is near the photosphere. It is, however, outside of our computation domain. The diffusion velocities in the wind region are assumed to be zero, which is consistent with the assumption of chemically homogeneous winds.

We calculate the radiative acceleration at the sonic point by use of the concept of force multipliers described by CAK and Abbott (1982) and various rough estimates. As no simple and reliable estimate for the occupation numbers in the wind region exists (Pauldrach 1987), the ones at $\overline{\tau} = \frac{2}{3}$ are assumed to be representative. The emergent fluxes from our own models described in Sect. 2 are used. The line list is the same as used for the diffusion calculations with 280 lines of the elements H, He, C, N and O, which are preferably the strongest lines. The justification for these assumptions is, that for solar composition and wind optical depths $\log t_{\rm e}$ smaller than about -5.5 our force multipliers coincide within a factor of about three with Abbott's ones. For the case of weak winds, which are of special interest for the present investigation, the densities at the sonic point are so low that according to our results $\log t_{\rm e} \approx -5.5$ is indeed an upper limit.

The maximum value of the force multiplier and thus the maximum radiative acceleration is reached for $\log t_{\rm e} \to -\infty$. Abbott (1982) has calculated force multipliers for $T_{\rm eff} \leq 50000$K and solar composition. At the smallest wind optical depth considered by him ($\log t_{\rm e} = -7$) the values are of the order 10^3. The dotted line in Fig. 1 would be maximum possible radiative acceleration, if the maximum value of the force multiplier were 10^3 for all effective temperatures. Thus only in the region above this line winds can exist. This result may be compared with the short-dashed line, which represents the corresponding wind limit obtained with the force multipliers from our calculations, where the occupation numbers at $\overline{\tau} = \frac{2}{3}$ for models with $\log g = 7$ have been used. For $T_{\rm eff} \leq 100000$K both estimates are of the same order. For $T_{\rm eff} > 100000$K, however, according to our results the maximum radiative acceleration even decreases with increasing $T_{\rm eff}$. This is because H and He are preferably fully ionized and the CNO elements have noble gas configuration, which makes the radiative acceleration small. The long-dashed line represents the wind limit for helium-rich composition with a solar ratio CNO/He. The long dashed-dotted line is the wind limit for PG 1159 stars with $\rm C/He = 0.3$, $\rm N/He = 0.01$ and $\rm O/He = 0.1$.

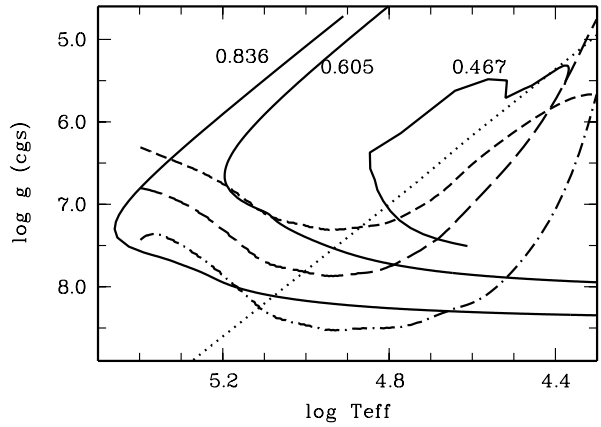

Fig. 1. The predicted wind limits in the $\log g$ - $\log T_{\rm eff}$ diagram for solar compostion (short dashed line), helium-rich composition with solar ratio CNO/He (long dashed), PG 1159 stars (dashed dotted) and for the case with a constant force multiplier of 10^3 (dotted line). In addition a $0.467 M_\odot$ post-EHB track from Dorman et al. (1993) and two post-AGB tracks from Blöcker (1995) are plotted

The results show that for hydrogen-rich white dwarfs with $M_* > 0.6 M_\odot$ the existence of chemically homogeneous winds is questionable for the whole cooling sequence. Only for less massive objects they may exist until they have reached a surface gravity of about $\log g = 7$. According to our results, for DO's the strong lines of $\rm He^+$ yield a major contribution to the total radiative acceleration. Mass loss possibly exists until they have cooled down to $T_{\rm eff} \approx 50000$K. As a consequence of their extremely large metal abundances, for PG 1159 stars the existence of winds is clearly more probable than for any other type of high-gravity stars. They are the only objects for which even at $\log g = 8$ mass loss may still exist.

We now estimate the mass loss rate from the conditions at the sonic point, where $v = a$. Then the right hand side of Eq. (34) must be zero. If the expression $\frac{2a^2}{r}$ is neglected, we have:

$$-g + g_{\rm rad,C} + g_{\rm rad,L}\left(\rho_{\rm s}, \frac{v_\infty}{R_*}, a\right) = 0. \qquad (35)$$

In general, the radiative acceleration due to bound-bound transitions, $g_{\mathrm{rad,L}}$, depends on the density, the gradient of the velocity and the velocity itself. From this equation the density ρ_{s} at the sonic point can be obtained, if an assumption about the velocity gradient is made. We use

$$\frac{dv}{dr} \approx \frac{v_\infty}{R_*}. \tag{36}$$

This assumption is motivated by the fact that for wind models calculated according to the CAK theory a β law is valid: $v_{(r)} = v_\infty \left(1 - \frac{r}{R_*}\right)^\beta$, where β is of the order 0.5. Then between $r = R_*$ and $r = 2R_*$ the velocity changes from $v \approx 0$ to $v \approx v_\infty$. To estimate the terminal velocity v_∞ we assume a constant ratio $v_\infty/v_{\mathrm{esc}}$

$$v_\infty \approx 3 v_{\mathrm{esc}} \tag{37}$$

where $v_{\mathrm{esc}} \approx \sqrt{2\frac{GM_*}{R_*}}$ is the escape velocity. According to the results for hot central stars of planetary neblue (Pauldrach et al. 1988), hot PG1159 stars (Koesterke et al. 1998) and main sequence B-stars (Babel 1996) this relation between v_{esc} and v_∞ should hold within a factor of two. With ρ_{s} from Eq. (35), the mass loss rate is obtained from the equation of continuity:

$$\dot{M} = 4\pi R_*^2 \rho_{\mathrm{s}} a. \tag{38}$$

5. The DAO/DA transition

In this section we investigate the question, for which hydrogen-rich white dwarfs mass loss prevents helium from sinking and when do they transform into DA's with no detectable helium. For the initial abundances of He and the CNO elements the solar ones are assumed. Evolutionary tracks for various masses are considered. A $0.414 M_\odot$ track from Driebe et al. (1998) represents the evolution of helium white dwarfs. They may be produced in binary systems, if the hydrogen-rich envelope is stripped away by a companion during the red giant branch phase. The remaining mass is too low for the ignition of helium burning. A $0.467 M_\odot$ track from Dorman et al. (1993) with a core mass $M_{\mathrm{c}} = 0.464 M_\odot$, a hydrogen envelope mass on the zero age horizontal branch $M^0_{\mathrm{env}} = 0.003 M_\odot$ and a mass fraction of metals $Z = 0.04$ has been chosen, because it passes through the region of the DAO's investigated by Bergeron et al. (1994). This track represents the evolution from the (extended) horizontal branch directly to the white dwarf region. Most of the DAO's analyzed by Napiwotzki (1999) have masses between 0.5 and $0.6 M_\odot$. Therefore we consider a $0.529 M_\odot$ post-early AGB track from Blöcker (1995) in detail. It represents the evolution of a star which suffers from two late helium flashes. At the cooling sequence, where we expect the onset of gravitational settling, this track is very similar to the $0.546 M_\odot$ post-AGB track from Schönberner (1983). However, for the latter data are available for $T_{\mathrm{eff}} > 70000$K only. In addition we consider various post-AGB tracks from Blöcker (1995) with masses between 0.605 and $0.836 M_\odot$.

The computations start before the star has reached its maximum effective temperature. This is sufficient, because during the preceding evolution the expected mass loss rates are usually large enough, so that the effect of diffusion is negligible. Exceptions are cases with $M > 0.6 M_\odot$. Here the wind limit may be reached even before the "knee" of the tracks, where they begin to cool. In Table 1 for various tracks the start values $T_{\mathrm{eff}(0)}$ and $\log g_{(0)}$ are given.

For $M_* = 0.529 M_\odot$, in Fig. 2 the surface composition is shown as a function of T_{eff}. The mass loss rates are obtained with the method described in Sect. 4, which allows for a dependance on the composition. They are plotted in Fig. 3 (solid line). The effect of gravitational settling is small until the star approaches the wind limit at $T_{\mathrm{eff}} = 90000$K, $\log g = 7.0$. Then mass loss cannot prevent or retard any longer the sinking of helium. As decreasing abundances of helium and heavy elements reduce the mass loss rate, we expect a rapid transformation of the DAO into a DA. The small discontinuities in the helium

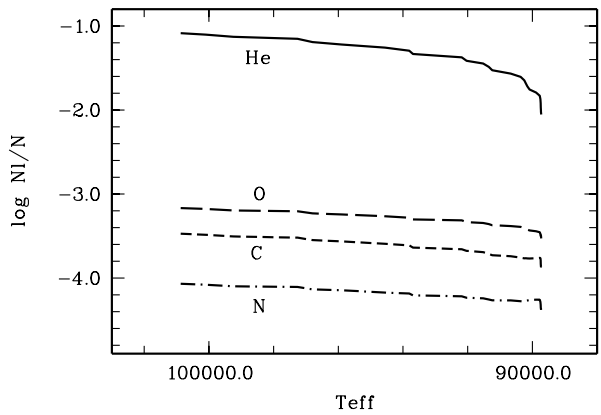

Fig. 2. Surface number fractions (number of particles of an element l over the total number of heavy particles) as a function of the effective temperature for the track with $M_* = 0.529 M_\odot$ and mass loss rates for which the dependence on the composition is taken into account

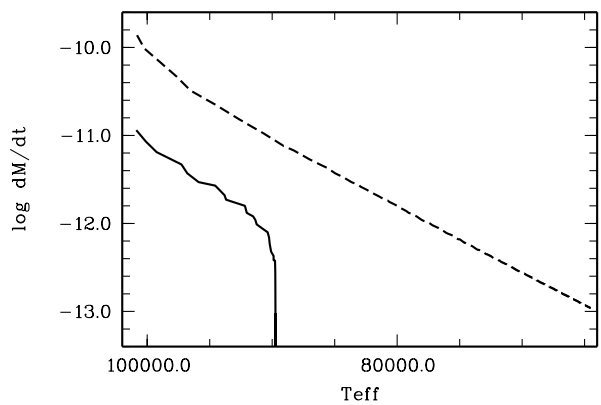

Fig. 3. Mass loss rates (in M_*/y, $M_* = 0.529 M_\odot$) according to this paper (solid line) and Eq. (33) (dashed line)

Table 1. Start values $T_{\mathrm{eff}(0)}$ and $\log g_{(0)}$ for various tracks

$M_*/M_\odot$	0.414	0.467	0.529	0.546	0.605	0.836
$T_{\mathrm{eff}(0)}$ [kK]	80.6	70.2	63.0	57.5	79.9	81.3
$\log g_{(0)}$ [cgs]	6.00	6.37	5.40	5.09	5.02	4.72

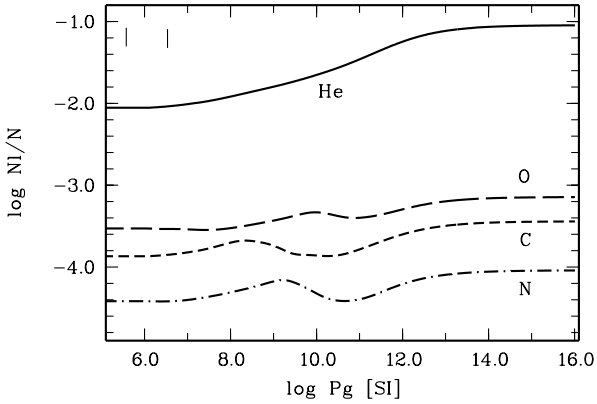

Fig. 4. Number fractions as a function of the gas pressure at $T_{\rm eff} = 90000$K, $\log g = 7.0$. In the upper part of the figure the Rosseland mean optical depths $\overline{\tau} = 1$ and 10 are indicated

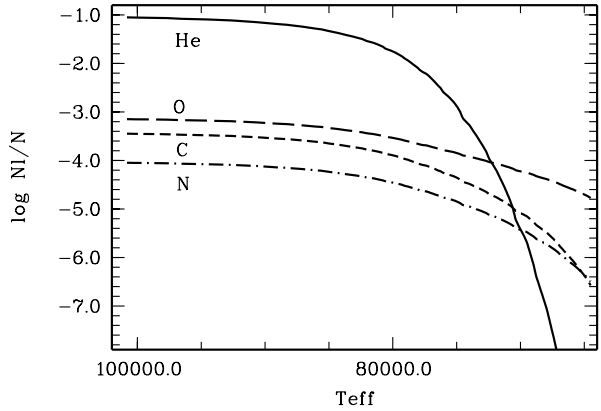

Fig. 5. Surface number fractions as a function of the effective temperature for the track with $M_* = 0.529 M_\odot$ and mass loss rates according to Eq. (33)

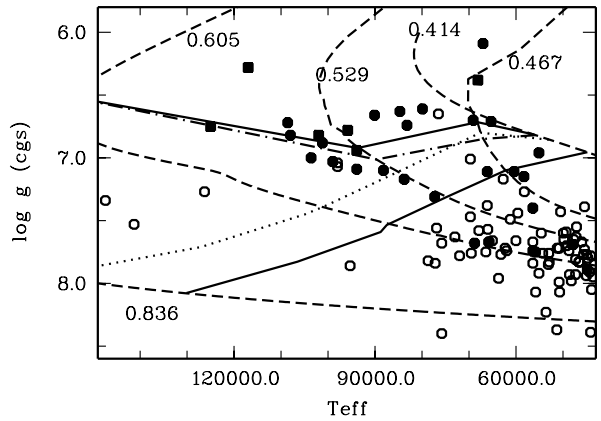

Fig. 6. Summary of the results in the $T_{\rm eff}$ - $\log g$ diagram. If the dependance of the mass loss rates on the composition is taken into account it is $\rm He/H = 0.05$ at the upper solid line and the wind limit is reached at the dashed-dotted line. With the rates from Eq. (33) it is $\rm He/H = 0.05$ at the dotted line and $\rm He/H = 10^{-3}$ at the lower solid line. The filled squares represent DAO's with $\rm He/H \approx 0.1$, the filled circles helium deficient DAO's and the open circles DA's, respectively. In addition several tracks are introduced (labelled with $M_*/M_\odot$)

abundance and mass loss rates appear because we update the mass loss rate only if the composition or the stellar parameters have changed by a certain amount (see Sect. 3.7). The CNO elements sink more slowly than helium. Whereas the number fraction of helium decreases by about a factor of ten in the range $100000\rm K \geq T_{\rm eff} \geq 90000\rm K$, the CNO elements are reduced by a factor of two only. The relative abundances of these elements are almost unchanged. At the wind limit the computations have been terminated. Perhaps selective winds still exist for a while, which lead to an outflow of such elements, for which the radiative force is large enough. Finally an equilibrium between gravitational settling and radiative levitation may be reached.

In Fig. 4 the number fractions of He, C, N and O are plotted as a function of the gas pressure for $T_{\rm eff} = 90000\rm K$, $\log g = 7.0$. Whereas the number fraction of helium continuously decreases from the inner to the outer regions, for the CNO elements we recognize the influence of the radiative acceleration, which acts especially on the hydrogen-like ions. For carbon this is near $\log P_{\rm g} \approx 10$, where the temperature is about $800000\rm K$. In regions where the radiative acceleration is very effective, the total velocity (diffusion + wind) has a local maximum. According to the equation of continuity this leads to a low particle density of the corresponding element. In the region with $\log P_{\rm g} < 9.0$ carbon preferably has helium-like configuration. The radiative acceleration and thus the total velocity decreases. This leads to an accumulation of carbon. So the abundance tends to have a minimum in regions where the radiative force is large and a maximum in the adjoining region where it is small. This situation is somewhat different as expected from diffusion calculations which assume an equilibrium between gravitational and radiative forces.

In Fig. 5 the surface composition is shown as a function of $T_{\rm eff}$, but now with the mass loss rates from Eq. (33). $\dot{M}$ is assumed to depend on the luminosity only. As the corresponding rates (dashed line in Fig. 3) are larger than those from our calculations, helium sinks later. At $T_{\rm eff} \approx 80000\rm K$ it is reduced by a factor of ten. Then the ongoing mass loss leads to a strong depletion of helium. The CNO elements sink more slowly. At $T_{\rm eff} \approx 65000\rm K$ they are reduced by a factor of 10 to 100, whereas no detectable helium is present. The helium abundance is even lower than predicted from the equilibrium diffusion calculations of Vennes et al. (1988). So in this scenario the DAO is transformed into a DA with an extremely low helium abundance, whereas the CNO elements are clearly less reduced. However, it requires that mass loss goes on independently of the low abundances.

In the $\log g$ - $T_{\rm eff}$ diagram of Fig. 6 the results obtained from the calculations along tracks with various masses are summarized. At the upper solid line the helium abundance would be reduced by a factor of two according to our mass loss calculations. So just before the tracks cross this line we expect the onset of gravitational settling. The dashed-dotted line is the wind limit. For all objects above this line, our results predict the existence of winds. After the onset of gravitational settling, the

wind limit is reached rapidly. Therefore both lines are close together. If the mass loss rates according to Eq. (33) are used, at the dotted line the helium abundance would be reduced by a factor of two. At the lower solid line would be He/H = 10^{-3}. In addition the DAO's analyzed by Napiwotzki (1999) and Bergeron et al. (1994) are shown (filled symbols), as well as the DA's (open symbols) from the compilation in Table A2 from Napiwotzki (1999). These objects, for which it is $\mathrm{He/H} \approx 0.1$ within the limits of uncertainty given by the authors, are represented by filled squares. In accordance with our results, they are preferably near or above the upper solid line, where the helium abundance should be reduced by not more than a factor of two. The objects below this line, for which the onset of gravitational settling is predicted, all are clearly helium deficient. In the region below the lower solid line both estimates predict the absence of helium, at least the abundance should be lower than 10^{-3}. Indeed, in the great majority of all hydrogen-rich white dwarfs in this region no helium has been detected. The few DAO's may either be influenced by accretion of matter (e.g. from a companion) or are possibly in a DO/DA transition state. For the two hottest known DA's (EGB 1 and WeDe 1) with $T_{\rm eff} \approx 145000$K and $\log g \approx 7.5$ Napiwotzki (1999) gives an upper limit $\mathrm{He/H} < 0.02$. From the estimate of the radiative acceleration in the wind region, we clearly expect the absence of mass loss. Therefore they should indeed be DA's. Eq. (33) yields a mass loss rate of the order 10^{-11}. Then, however, helium should be reduced by less than a factor of two and thus be detectable. This shows that $\dot{M} \approx 10^{-11}$ is an upper limit for these two objects.

If all progenitors of the white dwarfs had the same composition, the DAO's and DA's should be clearly separated in the $T_{\rm eff}$-$\log g$ diagram. Otherwise the mass loss rates will differ even for objects with the same mass. Therefore, in dependance of the initial composition, in some objects helium sinks earlier, in others later. This leads to the existence of a transition region, where DAO's as well as DA's with similar stellar parameters exist. Thus this coexistence of both types is not in contradiction to our results, but probably is a consequence of different evolutionary histories.

Napiwotzki (1999) found a relation between the helium abundance and the luminosity of hot DAO's. In Fig. 7 our predictions are shown. The solid lines represent the results obtained with the mass loss rates, for which the dependance on the composition is taken into account. The two left solid lines are the predictions for the tracks with 0.546 and $0.524 M_\odot$, respectively. As the tracks are similar, the results are similar, too. Therefore the two curves are close together. 16 out of 23 DAO's analyzed by Napiwotzki (1999) have masses in the range $0.48 \leq M_*/M_\odot \leq 0.58$ and are represented by circles in Fig. 7. The results show that they are close to our predictions. For objects with luminosities larger than $\approx 300 L_\odot$ the helium abundance is near the start value $\mathrm{He/H} = 0.1$. Here gravitational settling is negligible. To lower luminosities the helium abundance decreases slowly first, then there is a sharp cutoff at $L \approx 100 L_\odot$. The two right solid lines are the predictions for the 0.467 and 0.414 tracks, respectively. In these cases, the luminosities, for

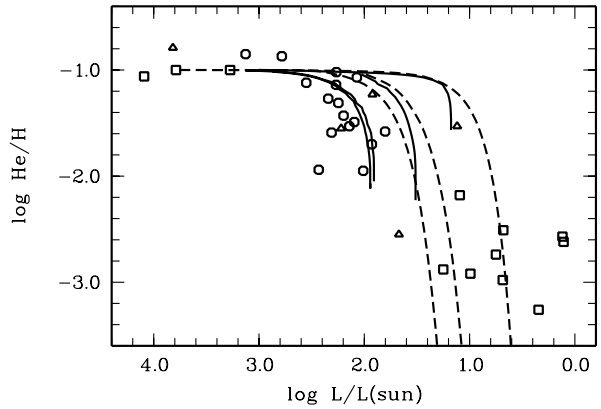

Fig. 7. The helium abundance as a function of the luminosity. The solid lines represent the predictions with mass loss rates from this paper for four tracks with (from left to the right) $M_* = 0.546, 0.524, 0.467$ and $0.414 M_\odot$, respectively. The dashed lines are the predictions with mass loss rates according to Eq. (33) for (from left to the right) $M_* = 0.605, 0.467$ and $0.414 M_\odot$. The DAO's from Napiwotzki (1999) with masses in the range $0.48 \leq M_*/M_\odot \leq 0.58$ are represented by circles, those with other masses by triangles. In addition the DAO's from Bergeron et al. (1994) are shown (squares)

which helium begins to sink, are lower. Most of the DAO's analyzed by Bergeron et al. (1994; represented by squares) have helium abundances in the range $-3.0 \leq \log n_{\rm He}/{\rm n_H} \leq -2.0$ and masses below $0.6 M_\odot$. According to our predictions they are beyond the wind limit. If the mass loss rates from Eq. (33) are used, however, for some of these DAO's an explanation with diffusion and mass loss seems to be still possible. The corresponding predictions for the tracks with 0.605, 0.467 and $0.414 M_\odot$ are represented by dashed lines. All these result show that at least in the luminosity range between about 10 and $300 L_\odot$ some relation between the helium abundance and the luminosity is indeed expected. A certain scatter will appear, if the various objects have very different masses and possibly initial compositions.

6. The PG 1159 / DO transition

In this section the transformation of PG 1159 stars into DO's will be investigated. An initial composition $\mathrm{C/He} = 0.3$, $\mathrm{N/He} = 0.01$ and $\mathrm{O/He} = 0.1$ (number ratios) and $\mathrm{H/He} = 0$ is assumed. Cases with hydrogen will be considered in the next section. The results for the $0.529 M_\odot$ born-again track from Blöcker (1995) are discussed in detail. This track is used, because the data for the corresponding 0.625 track are available for $T_{\rm eff} > 80000$K only and all known "cool" PG 1159 stars have masses smaller than about $0.7 M_\odot$.

In Fig. 8 the surface number fractions of the elements He, C, N and O are plotted as a function of $T_{\rm eff}$. The corresponding mass loss rates have been obtained with the method described in Sect. 4 and are shown in Fig. 9 (solid line). We see that mass loss with $\dot{M} \geq 10^{-12}$ effectively prevents the CNO elements from sinking. Until the star has cooled to $T_{\rm eff} = 65000$K the number fractions are reduced by a factor of about two only. Then,

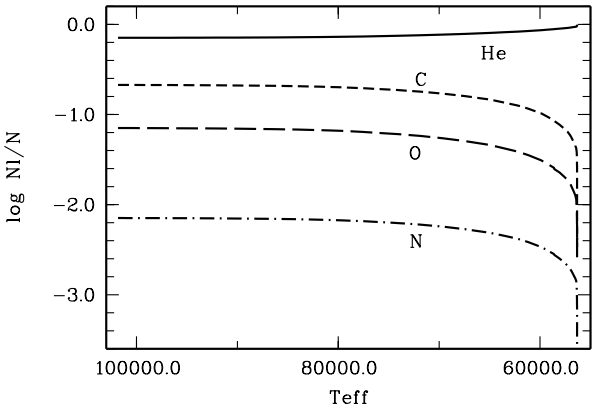

Fig. 8. Surface number fractions as a function of the effective temperature for the track with $M_* = 0.529 M_\odot$ and mass loss rates for which the dependance on the composition is taken into account

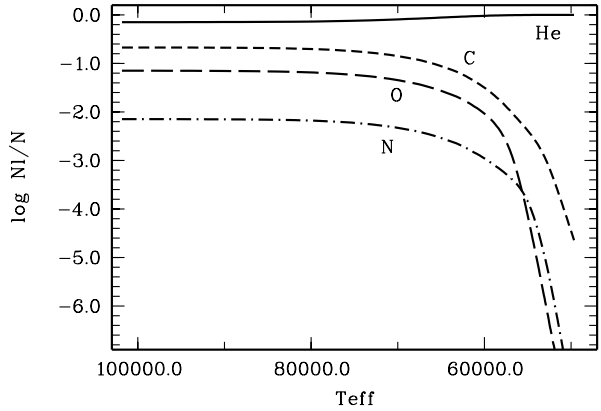

Fig. 10. Surface number fractions as a function of the effective temperature for the track with $M_* = 0.529 M_\odot$ and mass loss rates according to Eq. (33)

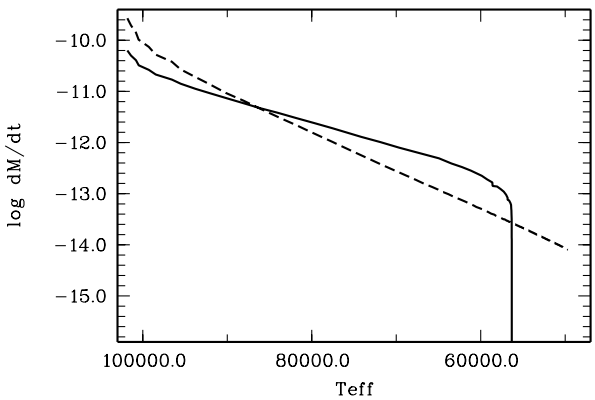

Fig. 9. Comparison of the mass loss rates (in M_*/y, $M_* = 0.529 M_\odot$) according to this paper (solid line) to the rates from Eq. (33)

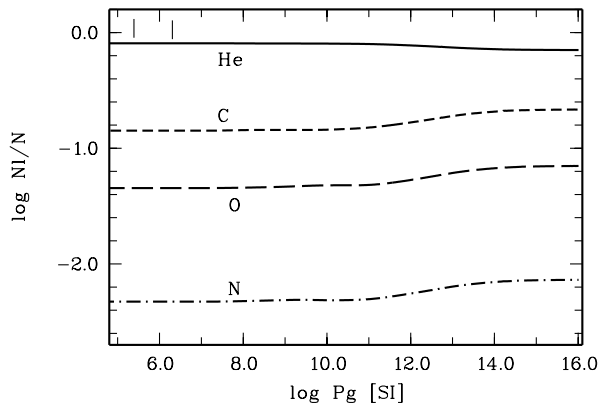

Fig. 11. Number fractions as a function of the gas pressure at $T_{\rm eff} = 70000$K, $\log g = 7.39$. In the upper part of the figure the Rosseland mean optical depths $\overline{\tau} = 1$ and 10 are indicated

as a consequence of the increasing gravity and the decreasing mass loss rates, the effect of gravitational settling becomes more and more apparent. Because of the ongoing depletion of heavy elements, finally the mass loss rate decreases drastically. At $T_{\rm eff} = 56300$K, the PG 1159 star is transformed into a DO. Here the CNO elements are reduced by about a factor of 20 and mass loss cannot exist any longer. During the cooling, the relative abundances of the CNO elements remain nearly unchanged. If an initial value of $\rm N/He = 10^{-5}$ instead of 0.01 is used, the results would be similar with the only difference that C and O sink somewhat earlier, because the mass loss rates are slightly lower. In this case the wind limit is reached at (at $T_{\rm eff} = 57400$K). The relative abundances of the CNO elements remain nearly unchanged. Therefore the signifcant differences of the nitrogen abundances in the various PG 1159 stars found by Dreizler & Heber (1998) cannot be due to diffusion processes.

For comparison, in Fig. 10 the corresponding results obtained with the mass loss rates according to Eq. (33) are shown. Again the PG 1159 star is transformed into a DO at $T_{\rm eff} \approx 60000$K with a somewhat smoother transition, however. This is because in this case $\dot{M}$ does not depend on the composition and decreases continiously (see Fig. 10). The ongoing mass loss beyond our predicted wind limit finally leads to a strong depletion of the CNO elements at $T_{\rm eff} \approx 50000$K.

It is a typical result that mass loss rates of the order 10^{-14} or somewhat lower lead to strong underabundances of the CNO elements. In depths where the temperature is between about 200000 and 400000K the CNO elements have noble gas configuration. The radiative acceleration is extremely small, which leads to negative diffusion velocities directed to the stellar interior. When the mass loss rate falls below a critical value, even the total velocity (diffusion+wind) may become negative. Thus the particles of these elements lost at the surface cannot be replaced any longer, because the supply from the stellar interior is interrupted. This is true for helium-rich as well as for hydrogen-rich white dwarfs.

In Figs. 11 and 12 the number fractions of the various elements are plotted as a function of the gas pressure for two examples. At $T_{\rm eff} = 70000$K, $\log g = 7.39$ (Fig. 11) the composition still is approximately homogeneous. The surface number fractions of the CNO elements are reduced by not more than a factor of two in comparison to the initial composition. The mass loss rates are of the order 10^{-12}. This is enough to prevent the formation of composition gradients. This is quite different from the

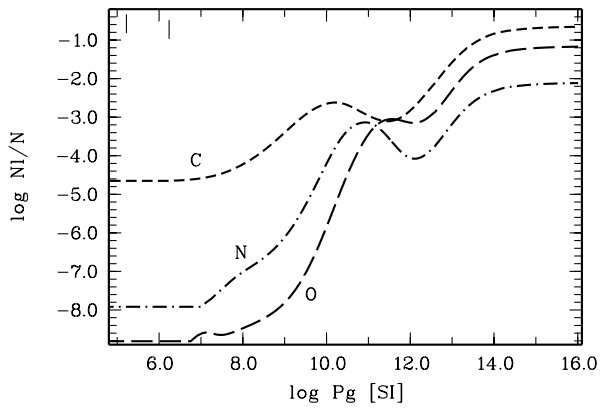

Fig. 12. The same as Fig. 11 at $T_{\rm eff} = 50000$K, $\log g = 7.62$

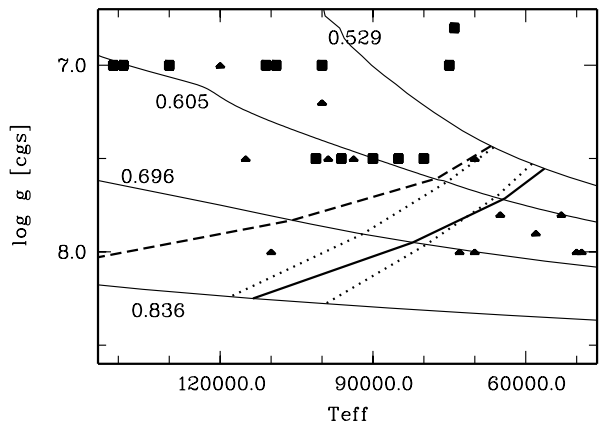

Fig. 13. Summary of the results in the $T_{\rm eff}$ - $\log g$ diagram. The solid line is the predicted wind limit for PG 1159 stars, the dashed line the wind limit obtained with mass loss rates reduced by a factor of 10. With the mass loss rates from Eq. (33) carbon would be reduced by a factor of two at the upper dotted line and by a factor of ten at the lower dotted line. The squares symbols represent PG 1159 stars, the triangles DO's. The thin lines represent the evolutionary tracks used for the computations (labelled with $M_*/M_\odot$)

situation at $T_{\rm eff} = 50000$K, $\log g = 7.62$ shown in Fig. 12. According to Eq. (33) it is $\dot{M} = 10^{-14}$ here. As explained above, this leads to strongly reduced abundances in the outer regions. At the stellar surface the number fraction of C is of the order 10^{-5}, these for N and O are even lower. Dreizler & Werner (1996) have analyzed several DO's with $T_{\rm eff} \approx 50000$K. Indeed, their upper limits for the abundances of the CNO elements are of the order 10^{-5}. This is lower than the predictions from the equilibrium diffusion theory, which is expected to be valid in the absence of mass loss or other competing processes. So the strong depletion of the CNO elements seems to be compatible with our predictions, if the mass loss rates are assumed to depend on the luminosity only. However, in the absence of heavy elements, chemically homogeneous winds could exist only if they were driven by the lines of helium alone. According to our estimate the radiative acceleration at the sonic point is too low (this would even be true for ratios $\rm CNO/He \approx 10^{-2}$). In addition we have estimated the radiative acceleration on helium at the sonic point for $T_{\rm eff} = 50000$K with the fluxes from a (static) NLTE model atmosphere with pure helium from Napiwotzki (priv. comm.). It is too low by a factor of the order 100. To summarize, an explanation of the low abundances of these DO's with diffusion and mass loss is possible. However, the driving mechanism of these winds is not clear.

In Fig. 13 all results of this section are summarized. Apart from the 0.529 track discussed above, we have done calculations for a 0.836 born-again track from Blöcker (1995). To cover the intermediate mass range two tracks for hydrogen burners have been used with $M_* = 0.605 M_\odot$ and $0.696 M_\odot$, respectively. The tracks for hydrogen and helium burners are very different during the pre-white dwarf evolution. On the cooling sequence, however, when we expect the onset of gravitational settling, they are similar. The surface gravities differ by a factor of about 1.2 only and the cooling ages are approximately the same.

Let us consider the two dotted lines in Fig. 13. With the mass loss rates from Eq. (33) carbon would be reduced by a factor of two at the upper dotted line and by a factor of ten at the lower one. Thus even if the dependance of the mass loss rate on the composition is neglected, we expect a narrow transition zone between PG 1159 stars and DO's. If we allow for a dependance of $\dot{M}$ on the composition, $\dot{M}$ decreases drastically when the heavy elements sink. This in turn favours gravitational settling so that we expect an even sharper transition. Therefore for these cases we have plotted the wind limit only, this is the line where we expect the transition. The solid line represents the wind limit if the mass loss rates from the method described in Sect. 4 are used. The dashed line is the wind limit from the same estimate, however with mass loss rates reduced by a factor of ten. The squares in Fig. 13 represent the PG 1159 stars from the list of Dreizler et al. (1995b), where the results of the new analyses of some objects by Dreizler & Heber (1998) have been taken into account. The triangles represent the DO's analyzed by Dreizler & Werner (1996). Clearly no PG 1159 star exists below the predicted transition region. Near a horizontal line at $\log g = 7.5$ several PG 1159 stars and DO's exist with similar stellar parameters. Some of these PG 1159 tendencially have somewhat lower abundances of C and O as it is typical for their hotter counterparts. This may be considered as an indication for the onset of gravitational settling. Two of the DO's (RE0503-289 with $T_{\rm eff} = 70000$K, $\log g = 7.5$ and PG0108+101 with $T_{\rm eff} = 95000$K, $\log g = 7.5$) have number ratios $\rm C/He \approx 0.01$. These abundances are clearly lower than in PG 1159 stars, but more than a factor of ten larger than the predictions from diffusion calculations without mass loss (Chayer et al. 1995a; Dreizler 1999). A natural explanation of these results is that they are transition objects. So from the observational side comes some evidence that the transition region is near a line with $\log g = 7.5$. If this line represents the transition region, this would require that our estimated mass loss rates are too large by more than a factor of ten. In Sect. 4 we have discussed the effect of line shadowing, which is of great importance in the case of thin winds. This may be one reason. Secondly, the densities in the wind region are much lower than at $\overline{\tau} = \frac{2}{3}$, where we have

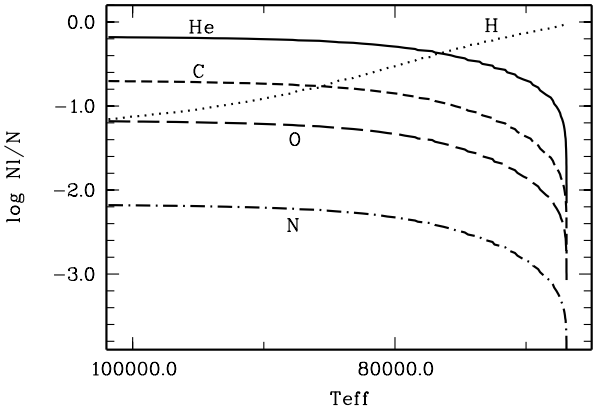

Fig. 14. Surface number fractions of H, He, C, N and O as a function of the effective temperature for the track with $M_* = 0.529 M_\odot$ and an initial number fraction $\frac{\mathrm{H}}{\mathrm{He}\,(0)} = 0.1$

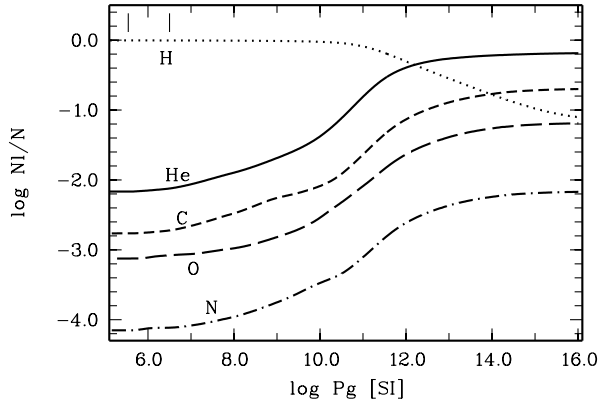

Fig. 15. Number fractions as a function of the gas pressure at $T_{\mathrm{eff}} = 67000\mathrm{K}$, $\log g = 7.43$ for the case with $\frac{\mathrm{H}}{\mathrm{He}\,(0)} = 0.1$. In the upper part of the figure the Rosseland mean optical depths $\overline{\tau} = 1$ and 10 are indicated

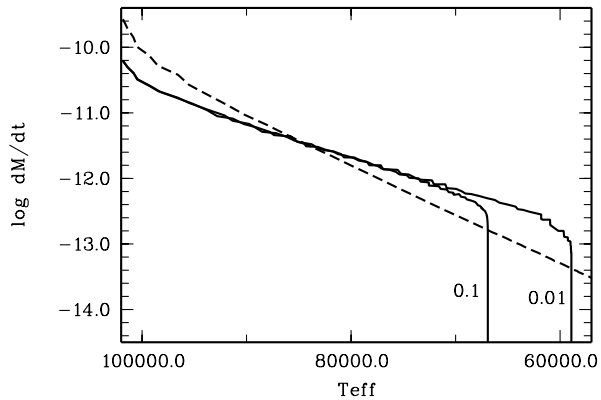

Fig. 16. Mass loss rates (in M_*/y; $M_* = 0.529 M_\odot$) as a function of the effective temperature. The two solid lines represent the rates obtained in this paper for the cases $\frac{\mathrm{H}}{\mathrm{He}\,(0)} = 0.1$ and 0.01, respectively. For comparison, the results from Eq. (33) are shown in addition (dashed line)

evaluated the occupation numbers. The lower densities favour higher ionization states such as He^{2+}, C^{4+}, N^{5+} and O^{6+}. For the CNO elements with helium-like configuration the radiative acceleration is low, however. For $T_{\mathrm{eff}} > 80000\mathrm{K}$ with increasing T_{eff} more and more particles tend to be in these ionization states. So it is well possible that the mass loss rates are approximately the same for objects with $80000\mathrm{K} \leq \mathrm{T_{eff}} \leq 120000\mathrm{K}$ and similar gravities, although the luminosities are very different. The estimates in Fig. 1 have shown that the maximum possible radiative acceleration in the wind region even tends to decrease for $T_{\mathrm{eff}} > 100000\mathrm{K}$. This could explain why in the T_{eff}-$\log g$ diagram the transition region is near a horizontal line with constant gravity.

According to our results the existence of PG 1159 and DO's with various composition with similar stellar parameters is not surprising, because we expect a sharp transition. Small differences in the initial composition may be the reason that the mass loss rates are somewhat different. Because of the resulting variations of the mass loss rates some objects may transform into DO's somewhat earlier, others later. So a certain overlap of the PG 1159 and DO region in the T_{eff} - $\log g$ diagram is expected and can even be considered as an indication for the existence of an evolutionary link between both types.

7. The floating up of hydrogen

In this section we again assume initial number ratios $\mathrm{C/He} = 0.3$, $\mathrm{N/He} = 0.01$, $\mathrm{O/He} = 0.1$, but now with various admixtures of hydrogen. For the track with $M_* = 0.529 M_\odot$ the results for initial ratios hydrogen $\frac{\mathrm{H}}{\mathrm{He}\,(0)} = 0.1$ and 0.2 will be discussed in detail. Then the results for all tracks are summarized.

In Fig. 14 the surface number fractions of the various elements are shown as a function of T_{eff} for an initial number ratio $\mathrm{H/He} = 0.1$. The corresponding mass loss rates are obtained with the method described in Sect. 4 and are shown in Fig. 16. For $T_{\mathrm{eff}} > 80000\mathrm{K}$ the results are similar as for the case without hydrogen discussed in the previous section. Mass loss with $\dot{M} > 10^{-12}$ keeps the stellar surface helium-rich and prevents the gravitational settling of the CNO elements. Then, at $T_{\mathrm{eff}} = 76000\mathrm{K}$ and $\log g = 7.3$, hydrogen floats up. The number fractions of the CNO elements are still reduced by a factor of two only, so that we now have a hybrid PG 1159 star. The enrichment of hydrogen in the outer regions favours the gravitational settling of the heavy elements. This is because the resistance coefficients in Eq. (2) are proportional to the square of the charge of the particles. This leads to larger diffusion velocities in hydrogen-rich surroundings in comparison to the helium-rich case. This has the consequence that in hydrogen-rich PG 1159 stars the heavy elements sink earlier than in helium-rich ones. For the example shown in Fig. 14 we expect the wind limit at $T_{\mathrm{eff}} = 67000\mathrm{K}$, $\log g = 7.43$. The corresponding internal structure is shown in Fig. 15. We now have a DAO with $\mathrm{He/H} \approx 10^{-2}$. Accidentally, N and O have nearly the solar abundance, only C is still somewhat overabundant. It seems to be impossible to find out spectroscopically, if such a DAO is in a transition state or a descendant from a hydrogen-rich progenitor. The tick marks in the upper left part in the figure indicate

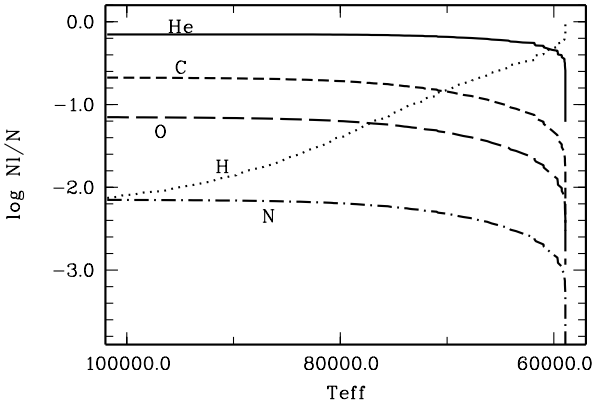

Fig. 17. Surface number fractions as a function of the effective temperature for the track with $M_* = 0.529 M_\odot$ and $\frac{\mathrm{H}}{\mathrm{He}\,(0)} = 0.01$

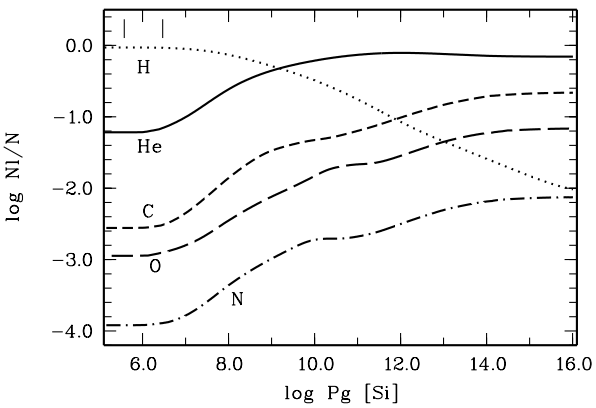

Fig. 18. Number fractions as a function of the gas pressure at $T_{\rm eff} = 58900$K, $\log g = 7.53$ and the case $\frac{\mathrm{H}}{\mathrm{He}\,(0)} = 0.01$. In the upper part of the figure the Rosseland mean optical depths $\overline{\tau} = 1$ and 10 are indicated

the mean optical depths $\overline{\tau} = 1$ and 10, respectively. It can be seen that the stellar atmosphere is in very good approximation chemically homogeneous.

In Fig. 17 the surface number fractions are shown as a function of $T_{\rm eff}$ for an initial ratio $\mathrm{H/He} = 0.01$, the corresponding mass loss rates are plotted in Fig. 16. Hydrogen floats up at $T_{\rm eff} = 60500$K, $\log g = 7.51$. Then the CNO elements sink rapidly and the wind limit is reached at $T_{\rm eff} = 58900$K, $\log g = 7.53$. So hydrogen floats up almost at the same time, when the CNO elements sink. The PG 1159 star directly evolves into a DAO, whereas the DO state is left out. In Fig. 18 the internal structure at the wind limit is shown. The outer regions are stratified with a hydrogen layer mass of about $10^{-11} M_*$ floating on top of the helium-rich regions. Again the stellar atmosphere is approximately chemically homogeneous, because during the transformation phase a weak wind is still present.

In Fig. 19 all results of this section are summarized. In addition we have done calculations for the tracks from Blöcker (1995) for $M_* = 0.605$ and $0.696 M_\odot$ (hydrogen burners) and $0.836 M_\odot$ (helium burners). The two dashed lines indicate where a number ratio $\mathrm{H/He} = 1$ is expected for initial ratios

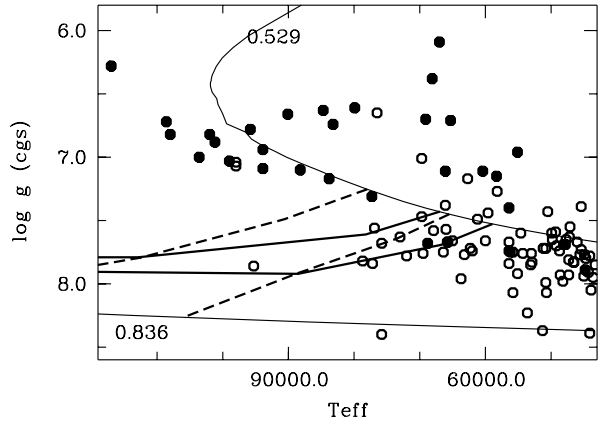

Fig. 19. Summary of the results in the $T_{\rm eff}$ - $\log g$ diagram. The dashed lines indicate, where (with $\dot{M}$ from Eq. (33)) it is $\mathrm{H/He} = 1$ for initial ratios $\frac{\mathrm{H}}{\mathrm{He}\,(0)} = 0.1$ (upper line) and 0.01 (lower line). The solid lines indicate the wind limits for both cases, derived with $\dot{M}$ from this paper (the upper line is for $\frac{\mathrm{H}}{\mathrm{He}\,(0)} = 0.1$, the lower line for 0.01, respectively). In addition are introduced the same DAO's (filled symbols) and DA's (open symbols) as in Fig. 6 and two evolutionary tracks labelled with the mass in $M_\odot$

$\frac{\mathrm{H}}{\mathrm{He}\,(0)} = 0.1$ and 0.01, respectively. These two lines have been derived with the mass loss rates from Eq. (33). (The corresponding results obtained with the mass loss rates from this paper are similar, they are shown in Fig. 20.) With the rates according to this paper we expect the wind limit for the two cases at the solid lines in Fig. 19. So PG 1159 stars with an initial number ratio $0.01 \leq \frac{\mathrm{H}}{\mathrm{He}\,(0)} \leq 0.1$ will transform into DAO's somewhere near the region between the upper dashed line and the lower solid line. For $\frac{\mathrm{H}}{\mathrm{He}\,(0)} < 0.01$ the results would be very similar to the case without hydrogen discussed in the previous section. The heavy elements sink and the wind limit is reached before hydrogen floats up. So only these PG 1159 stars will be transformed into DO's.

The most important conclusion from the results shown in Fig. 19 is, that the majority of all DAO's cannot be descendants of hydrogen-poor PG 1159 stars with $\frac{\mathrm{H}}{\mathrm{He}\,(0)} \leq 0.1$. This is true especially for objects with $\log g \approx 7$ or even lower surface gravities. For the expected mass loss rates hydrogen would not yet float up. The DAO's with $M_* \leq 0.5 M_\odot$ probably have evolved directly from the extented horizontal branch (EHB) to the white dwarf region. Thus they are descendants from sdB, sdOB or sdO stars (for a review see Heber 1992). The H/He ratio of these objects varies from helium-poor with $\mathrm{H/He} \approx 10^{-5}$ to helium-rich with no detectable hydrogen. Although in this section we have not investigated the post-EHB evolution, it is plausible that these variations have consequences for the composition of the corresponding white dwarfs.

8. Summary and conclusions

In the $\log g$-$T_{\rm eff}$ diagram the white dwarfs evolve from a region where winds exist into a region where no winds exist. Therefore somewhere on the cooling sequence mass loss must terminate,

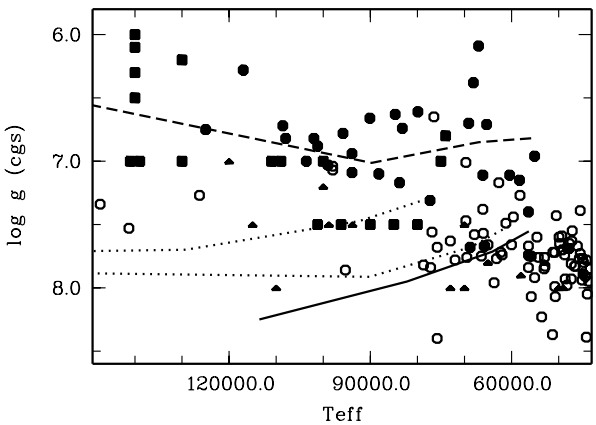

Fig. 20. Summary of the results in the $T_{\rm eff}$-$\log g$ diagram. The dashed line represents the wind limit for hydrogen-rich white dwarfs. Near this line we expect the transition from DAO's into DA's. The solid line is the wind limit for PG 1159 stars, which can exist above this line only. For PG 1159 stars with an initial ratios $\rm H/He \leq 0.1$ and 0.01, we expect the floating up of hydrogen ($\rm H/He = 1$) at the upper and lower dotted line, respectively. The filled circles represent the DAO's from Napiwotzki (1999) and Bergeron et al. (1994), the open symbols the DA's from the compilation of Napiwotzki (1999). The filled squares represent the PG 1159 stars from Dreizler et al. (1995b) and Dreizler & Heber (1998), the triangles the DO's from Dreizler & Werner (1996)

this is the wind limit. When the white dwarfs approach the wind limit and the mass loss rate decreases below about 10^{-11} we expect the onset of gravitational settling. The heavy elements (and helium in hydrogen-rich white dwarfs) begin to sink slowly. During the ongoing cooling the surface gravity increases. This and the decreasing abundances of heavy elements (and helium) favour the diminution of the mass loss rates. Then the elements sink rapidly and, for example, DAO's transform into DA's or PG 1159 stars into DO's. In Fig. 20 the most important results are summarized. The dashed line near $\log g = 7$ represents the wind limit for hydrogen-rich white dwarfs. These DAO's, which had approximately solar composition before they entered the cooling sequence, should transform into DA's near this line. This is in good agreement with the observational results. With one exception, in all objects above this line helium has been detected, whereas below more and more DA's appear. If the mass loss rates obtained from the two estimates used in our calculations are of the correct order of magnitude, the majority of the DAO's cannot be descendants of hydrogen-poor PG 1159 stars. For initial ratios $\rm H/He \leq 0.1$ and 0.01 hydrogen floats up near the upper and lower dotted line, respectively. Dreizler & Werner (1996) report on an increasing ratio of hydrogen- to helium-rich white dwarfs with decreasing $T_{\rm eff}$. This result is expected, if their progenitors have a continuous distribution of H/He ratios with a variety of metal abundances.

For PG 1159 stars with initial H/He ratios below 0.01, according to our results the wind limit is between about $\log g = 7.5$ and 8.0 (solid line in Fig. 20). Near this line PG 1159 stars with an initial composition $\rm C/He = 0.3$, $\rm N/He = 0.01$ and $\rm O/He = 0.1$ (number ratios) should be transformed into DO's. In agreement with this prediction, no PG 1159 star exists below this line. From the results in Sect. 6 we have seen that during the cooling the CNO elements first sink very slowly and then we expect a sharp transition into a DO. Because the initial compositions and thus the mass loss rates of the various objects may differ, an overlap of the regions populated by PG 1159 and DO's must be expected. Therefore the existence of PG 1159 stars and DO's with similar stellar parameters near a line with $\log g = 7.5$ is consistent with the existence of an evolutionary link. This implies that the majority of the DO's may belong to an evolutionary sequence which leads from the helium- and carbon-rich central stars of planetary nebulae (spectral type [WC]) via the PG 1159 phase into the DO white dwarfs. It is not clear, however, if this is true for all ones. Rauch et al. (1998) analyzed several helium -rich pre-white dwarfs (O(He) stars) in the range $100000\rm K \leq T_{\rm eff} \leq 140000\rm K$, $5.5 \leq \log g \leq 6.5$, which do not show the strong lines of carbon typical for PG 1159 stars. This may be an indication for the existence of a distinct sequence, which never passes through the PG 1159 phase.

In Sect. 7 we have shown that PG 1159 stars with initial number ratios $\rm H/He \geq 10^{-2}$ directly evolve into DAO's, whereas the DO phase is left out. During the floating up of hydrogen some mass loss may still be present, so that the stellar atmosphere is in good approximation chemically homogeneous. According to Paper I weak winds with $\dot{M} \geq 10^{-16}$ prevent the development of an equilibrium between gravitational settling and concentration gradients. Stratified H/He atmospheres as calculated by Jordan & Koester (1986) or Vennes & Fontaine (1992) can exist only in the absence of any significant mass loss. PG 1159 stars which have initial ratios $\rm H/He \ll 10^{-2}$ transform into DO's. Due to the decreasing metal abundances we expect the termination of mass loss. In the absence of mass loss, however, hydrogen should float up rapidly. In Paper I it has been shown, that a DO with an initial ratio $\rm H/He = 10^{-4}$ may evolve into a DA within a time scale of 10^4 to $10^5\rm y$. In cooling DO's, at $T_{\rm eff} \approx 65000\rm K$ helium recombination leads to the formation of an outer convection zone (Tassoul et al. 1990) with a mass of less than $10^{-14} M_*$. If, in the presence of a wind, the mass within this zone is lost rapidly, the influence of convection is negligible. When the mass loss rate approaches zero, convection may somewhat prolong the time scales, in which the surface composition changes. However, as diffusion acts in regions below, this thin convection zone probably cannot prevent the floating up of hydrogen. So we expect that finally all helium-rich white dwarfs evolve into DA's, if any traces of hydrogen are present. From these arguments it is plausible that in the $T_{\rm eff}$-$\log g$ diagram below the wind limit a region exist where all white dwarfs are DA's. This scenario could be a possible explanation for the existence of the DB-gap, if mass loss terminates for all white dwarfs before they have reached the blue end near $T_{\rm eff} = 45000\rm K$. It fits into this picture that the only DAO of the sample of Bergeron et al. (1994), which shows evidence for stratification (PG 1305-017) is with $T_{\rm eff} = 44400\rm K$ indeed one of the coolest ones. The existence of a stratified atmosphere is a clear indication for the absence of mass loss.

For a detailed comparison of the theoretical predictions with the abundances of individual objects a precise knowledge of the

mass loss rates would be required. Diffusion calculations which assume an equilibrium between gravitational settling and radiative levitation are appropriate only in the absence of mass loss or if at least $\dot{M} \ll 10^{-16}$. This has been shown in Paper I for mixtures of hydrogen and helium and by Chayer et al. (1997) for the case of silicon in DA's. An example is G 191-B2B with $T_{\rm eff} = 56000$K, $\log g = 7.6$ (Wolff et al. 1998). Dreizler & Wolff (1999) analyzed the ultraviolet and extreme-utraviolet spectra using self-consistent diffusion models. The results can reproduce the flux distribution and the ultraviolet lines at least of iron. The abundance distribution in the atmosphere is stratified, a result which has also been suggested by Barstow et al. (1999). So for DA's equilibrium diffusion calculations seem to be promising. This is consistent with our results, which predict the absence of mass loss in DA's with $\log g > 7$, especially if the abundances of the heavy elements are clearly below the solar one. For DO's the diffusion calculations of Dreizler (1999) cannot explain the observed spectra, they can best be fitted with chemically homogeneous models. From the calculations presented in this paper and from previous calculations with fixed $T_{\rm eff}$ and $\log g$ we obtain the following results. For DO's with mass loss rates in the range $10^{-14} \leq \dot{M} \leq 10^{-12}$ the surface composition is more or less affected by gravitational settling. However, the CNO elements should still be present. Therefore the hotter DO's analyzed by Dreizler (1999) should have mass loss rates within this range, if they are descendants of PG 1159 stars and thus the composition is a consequence of gravitational settling. Abundances of the CNO elements of 10^{-5} and lower as found in the two cooler DO's HZ 21 and HD 149499 B with $T_{\rm eff} \approx 50000$K and $\log g \approx 8$ are expected only for $\dot{M} < 10^{-14}$. Therefore for these two DO's 10^{-14} is an upper limit for the mass loss rate. These result support the hypothesis that for DO's near the blue end of the DB-gap the mass loss rate approaches to zero, which favours the floating up of hydrogen. In addition, the results indicate that in DO's winds more probably exist rather than in DA's. However, the driving mechanism still has to be investigated in detail.

Acknowledgements. We thank R. Napiwotzki and the referee for carefully reading the manuscript and useful comments.

References

Abbott D.C., 1982, ApJ 259, 282
Babel J., 1995, A&A 301, 823
Babel J., 1996, A&A 309, 867
Barstow M.A., Hubeny I., Holberg J.B., 1999, A.S.P. Conf. Ser. 169, 479
Bergeron P., Wesemael F., Beauchamp A., et al., 1994, ApJ 432, 305
Blöcker T., 1995, A&A 299, 755
Blöcker T., 2000, in: Blöcker T., Waters L.B.F., Zijlstra A.A. (eds.), Low mass Wolf-Rayet stars: Origin and evolution, Astrophysics and Space Science, in press
Blöcker T., Herwig F., Driebe T., Bramkamp H., Schönberner D., 1997, in: Isern J., Hernanz M., Garcia-Berro E. (eds.), White Dwarfs. Kluwer Academic Publishers, p. 57
Castor J.I., Abbott D.C., Klein R.I., 1975, ApJ 195, 157
Chayer P., Fontaine G., Wesemael F., 1995a, ApJS 99, 189
Chayer P., Vennes S., Pradhan A.K., et al., 1995b, ApJ 454, 429
Chayer P., Fontaine G., Pelletier C., 1997, in: Isern J., Hernanz M., Garcia-Berro E. (eds.), White Dwarfs, Kluwer Academic Publishers, p. 253
Dorman B., Rood R.T., O'Connell R.W., 1993, ApJ 419, 596
Deetjen J.L., Dreizler S., Rauch T., Werner K., 1999, A&A 348, 940
Dreizler S., 1999, A&A 352, 632
Dreizler S., Heber U., 1998, A&A 334, 618
Dreizler S., Werner K., 1996, A&A 314, 217
Dreizler S., Wolff B., 1999, A&A 348, 189
Dreizler S., Heber U., Napiwotzki R., Hagen H.-J., 1995a, A&A 303, L53
Dreizler S., Werner K., Heber U., 1995b, in: Koester D., Werner K. (eds.), White Dwarfs, Lecture Notes in Physics 443, p. 160
Driebe T., Schönberner D., Blöcker T., Herwig F., 1998, A&A 339, 123
Fontaine G., Wesemael F., 1987, IAU Coll. 95, in: Phillip A.G.D., Hayes D.S., Liebert J. (eds.), The Second Conference on Faint Blue Stars, Davis Press, p.285
Fontaine G., Wesemael F., 1997, in: Isern J., Hernanz M., Garcia-Berro E. (eds.), White Dwarfs, Kluwer Academic Publishers, p. 173
Hawley J.F., Smarr L.L., Wilson J.R., 1984, ApJS 55, 211
Heber U., 1992, in: Heber U., Jeffery C.S. (eds.), The Atmospheres of Early-Type Stars, Springer Verlag, p. 234
Herwig F., Blöcker T., Langer N., Driebe T., 1999, A&A 349, L5
Holberg J.B., Barstow M.A., Sion E.M., 1998a, ApJS 119, 207
Holberg J.B., Barstow M.A., Sion E.M., 1998b, in: Philip A.G.D., Liebert J., Saffer R.A. (eds.), The Third Conference on Faint Blue Stars, Davis Press, p. 331
Holberg J.B., Barstow M.A., Sion E.M., 1999, A.S.P. Conf. Ser. 169, 485
Iben I.Jr., Kaler J.B., Truran J.W., Renzini A., 1983, ApJ 264, 605
Jordan S., Koester D., 1986, A&AS 65, 367
Koester D., Wolff B., Jordan S., Dreizler S., 1998, in: Philip A.G.D., Liebert J., Saffer R.A. (eds.), The Third Conference on Faint Blue Stars, Davis Press, p. 313
Koesterke L., Werner K., 1998, ApJ 500, L55
Koesterke L., Dreizler S., Rauch T., 1998, A&A 330, 1041
Kudritzki R.P., Méndez R.H., Puls J., McCarthy J.K., 1997, in: Habing H.J., Lamers H.J.G. (eds.), Planetary Nebulae, IAU Symp. 180, p. 64
Massacrier G., 1996, A&A 309, 979
Méndez R.H., 1991, in: Michaud G., Tutukov A. (eds.), Evolution of stars: The photospheric abundance connection, IAU Symp. 145, p. 375
Mihalas D., 1978, Stellar Atmospheres 2nd ed., San Francisco: Freeman
Napiwotzki R., 1999, A&A 305, 101
Napiwotzki R., Schönberner D., 1991, A&A 249, L16
Napiwotzki R., Schönberner D., 1993, in: Barstow M.A. (ed.), White Dwarfs: Advances in Observation and Theory, NATO ASI Series 403, p. 99
Napiwotzki R., Schönberner D., 1995, A&A 301, 545
Paquette C., Pelletier C., Fontaine G., Michaud G., 1986a, ApJS 61, 177
Paquette C., Pelletier C., Fontaine G., Michaud G., 1986b, ApJS 61, 197
Pauldrach A., 1987, A&A 183, 295
Pauldrach A., Puls J., Kudritzki R.P., Méndez R.H., Heap S.R., 1988, A&A 207, 123
Perinotto M., 1993, IAU Symp. 55, p.57

Rauch T., Dreizler S., Wolff B., 1998, A&A 338, 651
Rauch T., Köppen J., Napiwotzki R., Werner K., 1999, A&A 347, 169
Schönberner D., 1983, ApJ 272, 708
Tassoul M., Fontaine G., Winget D.E., 1990, ApJS 72, 335
Unglaub K., Bues I., 1996, A&A 306, 843
Unglaub K., Bues I., 1997, A&A 321, 485
Unglaub K., Bues I., 1998, A&A 338, 75 (Paper I)
Unglaub K., Bues I., 1999, A.S.P. Conf. Ser. 169, 422
Vauclair G., Vauclair S., Greenstein J.L., 1979, A&A 80, 79
Vennes S., Fontaine G., 1992, ApJ 401, 288
Vennes S., Pelletier C., Fontaine G., Wesemael F., 1988, ApJ 331, 876
Werner K., 2000, in: Blöcker T., Waters L.B.F., Zijlstra A.A. (eds.), Low mass Wolf-Rayet stars: Origin and evolution, Astrophysics and Space Science, in press
Werner K., Dreizler S., Heber U., et al., 1995, A&A 293, L75
Werner K., Dreizler S., Rauch T., et al., 1999, A.S.P. Conf. Ser. 169, 511
Wolff B., Koester D., Dreizler S., Haas S., 1998, A&A 329, 1045